Wind and Structures, Vol. 7, No. 3 (2004) 187-202
DOI: http://dx.doi.org/10.12989/was.2004.7.3.187

Identification of eighteen flutter derivatives of an airfoil and a bridge deck

Arindam Gan Chowdhury† and Partha P. Sarkar‡

Department of Aerospace Engineering, Iowa State University, 2271 Howe Hall, Ames, Iowa, 50011-2271, USA
(Received October 1, 2003, Accepted February 12, 2004)

Abstract. Wind tunnel experiments are often performed for the identification of aeroelastic parameters known as flutter derivatives that are necessary for the prediction of flutter instability for flexible structures. Experimental determination of all the eighteen flutter derivatives for a section model facilitates complete understanding of the physical mechanism of flutter. However, work in the field of identifying all the eighteen flutter derivatives using section models with all three degree-of-freedom (DOF) has been limited. In the current paper, all eighteen flutter derivatives for a streamlined bridge deck and an airfoil section model were identified by using a new system identification technique, namely, Iterative Least Squares (ILS) approach. Flutter derivatives of the current bridge and the Tsurumi bridge are compared. Flutter derivatives related to the lateral DOF have been emphasized. Pseudo-steady theory for predicting some of the flutter derivatives is verified by comparing with experimental data. The three-DOF suspension system and the electromagnetic system for providing the initial conditions for free-vibration of the section model are also discussed.

Keywords: system identification; elastic suspension system; flutter derivatives; wind tunnel testing; pseudo-steady theory.

1. Introduction

Aeroelasticity refers to the phenomenon wherein aerodynamic forces and structural motions interact significantly. Flutter is a self-excited oscillation of a structural system that occurs due to aeroelastic interaction. Flutter speed and frequency of a structure can be calculated by a frequency-domain method using flutter derivatives that are experimentally obtained from wind-tunnel testing of section models (Scanlan 1978). Sarkar, Jones, and Scanlan (1994) were successful in identifying eight flutter derivatives simultaneously from noisy displacement time histories by modified Ibrahim time domain (MITD) method. Brownjohn and Jakobsen (2001) used Covariance block Hankel matrix (CBHM) method for parameter extraction of a two-degree-of-freedom (DOF) system. The CBHM method was also extended to cater for three-DOF, however, the principles were illustrated for a two-DOF system and eight flutter derivatives were experimentally extracted. Gu, Zhang, and Xiang (2000) and Zhu, *et al.* (2002) used an identification method based on unifying least squares (ULS) theory to extract flutter derivatives of a two-DOF model. Although the ULS method could theoretically identify all the eighteen flutter derivatives using a three-DOF section model, only eight

† Graduate Research Assistant
‡ Associate Professor and Wilson Chair

flutter derivatives were extracted due to lack of a more inclusive experimental setup to accommodate the three-DOF section model.

Identification of all the eighteen flutter derivatives of a streamlined bridge deck was first attempted by Singh, *et al.* (1995). They extended the MITD method developed by Sarkar, Jones, and Scanlan (Sarkar 1992). The trends of some of the indirect flutter derivatives, namely, $H6^*$, $A5^*$, $A6^*$, $P3^*$, $P5^*$, and $P6^*$, are difficult to predict due to the scatter in the data presented in the plots by Singh, *et al.* (1995); for the other flutter derivatives, specific trends are evident from the plots. Chen, He, and Xiang (2002) used general least-squares theory for identifying eighteen flutter derivatives of bridge sections. Experimental results were compared to results from computational fluid dynamics (CFD) methods. At lower reduced velocities, the experimental results were consistent with the CFD results for the lateral flutter derivatives. At higher velocities, the results of most lateral derivatives differed between both approaches. When comparing two-DOF and three-DOF sectional model experiments, good agreement was found for flutter derivatives $H1^*$, $H2^*$, $H3^*$, $A1^*$, $A2^*$, $A3^*$, but deviations were noted for $H4^*$ and $A4^*$.

It is evident from the literature mentioned above that the work in the field of identifying all the eighteen flutter derivatives for section models is limited and needs further investigation. Efficient extraction of all the eighteen flutter derivatives requires an effective system identification technique and a versatile three-DOF elastic suspension system. This motivated the development of a new system identification method and a versatile three-DOF elastic suspension system which together are capable of efficiently extracting all the eighteen flutter derivatives for section models involving different DOF-combination testing. The current paper describes their implementation for extraction of eighteen flutters derivatives for an airfoil and a bridge deck section model and it mainly highlights the results of flutter derivatives related to the lateral DOF. The system identification method involves digital filtering of noisy displacement time histories and numerically generating their higher derivatives (velocity and acceleration) using finite difference formulation. The current formulation has the following advantages – (i) a single computer program is capable of extracting flutter derivatives for various DOF combination cases (e.g., 1-DOF, 2-DOF, and 3-DOF cases), (ii) effective stiffness and damping matrices are directly obtained from acquired free-vibration displacement time histories and numerically generated velocity and acceleration time histories using digital filtering and finite differencing (thus avoiding extraction of eigenvalues and eigenvectors), and (iii) accurate parameter identification can be performed, as has been validated numerically and experimentally, where different DOF combinations were used.

2. Iterative Least Squares (ILS) system identification method

Experimentally obtained flutter derivatives are used for flutter analysis in the frequency domain. In this formulation, the aeroelastic forces acting on a structure are modeled by means of flutter derivatives. For a three-DOF section model, the three degrees of freedom are the vertical deflection, h, and the horizontal deflection, p, of the local center-of-gravity (*c.g.*), and the rotation, α, about that *c.g.*

A new system identification technique that uses iterative least squares approach has been developed for the extraction of flutter derivatives from free vibration displacement time histories obtained from a section model testing in the wind tunnel. The method will be referred hereafter as the Iterative Least Squares (ILS) method. The aeroelastically-modified equations of motion can be represented as the state-space model:

$$\dot{\underline{X}} = \underline{A}\underline{X} \quad \text{where, } \underline{X} = \begin{Bmatrix} \underline{y} \\ \dot{\underline{y}} \end{Bmatrix}, \ \underline{y} = \{h \ \alpha \ p\}^T, \ \underline{A} = \begin{bmatrix} \underline{0} & \underline{I} \\ -\underline{K}^{eff} & -\underline{C}^{eff} \end{bmatrix} \tag{1}$$

The $\underline{A}$ matrix is a $2n \times 2n$ square matrix, where n is the number of degree of freedom for the dynamic system and $\underline{I}$ is the identity matrix of size $n \times n$. $\underline{C}^{eff}$ and $\underline{K}^{eff}$ are the aeroelastically modified effective damping and stiffness matrices, respectively, that include the aeroelastic force vector components (aeroelastic lift L_{ae}, moment M_{ae}, and drag D_{ae}) written as follows (Scanlan and Jones formulation as in Sarkar 1992):

$$\underline{F}_{ae} = \begin{Bmatrix} L_{ae} \\ M_{ae} \\ D_{ae} \end{Bmatrix} = \begin{bmatrix} 0.5\rho U^2 B & 0 & 0 \\ 0 & 0.5\rho U^2 B^2 & 0 \\ 0 & 0 & 0.5\rho U^2 B \end{bmatrix}$$

$$\cdot \begin{bmatrix} KH_1^*/U & KH_2^*B/U & KH_5^*/U & K^2H_4^*/B & K^2H_3^* & K^2H_6^*/B \\ KA_1^*/U & KA_2^*B/U & KA_5^*/U & K^2A_4^*/B & K^2A_3^* & K^2A_6^*/B \\ KP_5^*/U & KP_2^*B/U & KP_1^*/U & K^2P_6^*/B & K^2P_3^* & K^2P_4^*/B \end{bmatrix} \begin{Bmatrix} \dot{h} \\ \dot{\alpha} \\ \dot{p} \\ h \\ \alpha \\ p \end{Bmatrix} \tag{2}$$

where, ρ is the air density; U is the mean cross wind velocity; $K = B\omega/U$ is the non-dimensional reduced frequency; ω is the circular frequency of oscillation.

The non-dimensional aerodynamic coefficients H_i^*, P_i^*, and A_i^* ($i = 1, 2, ..., 6$) are called the flutter derivatives and they evolve as functions of the reduced velocity U/fB (where $f = \omega/2\pi$ is the frequency of oscillation). These coefficients can be determined from wind-tunnel experiments on section models excited by initial displacements.

The $\underline{A}$ matrix in Eq. (1) can be identified if displacement ($\underline{y}$), velocity ($\dot{\underline{y}}$), and acceleration ($\ddot{\underline{y}}$) data can be recorded for all n degree of freedom for at least $2n$ different instants of time (Ibrahim and Mikulcik 1976). Practically, measurement of all three responses is not feasible so an alternate procedure has been formulated. In this procedure, the noisy displacement time histories are only measured and filtered numerically to remove the high frequency noise components (if any). MATLAB is used for zero-phase digital filtering of the noisy displacement time history and a low-pass digital 'Butterworth' filter is programmed for this purpose. The cutoff frequency for the filter can be estimated from the knowledge of approximate zero-wind speed frequencies of the dynamic system. This filtered displacement data are then used to generate velocity and acceleration time histories by finite difference formulation. The digitally filtered displacement and the numerically obtained velocity and acceleration time histories deviate from the actual time histories at the two extreme ends of the total time range. This is an inherent error for zero-phase digital filtering using MATLAB function. To circumvent the misfit at the two ends, a 'windowing' method was applied,

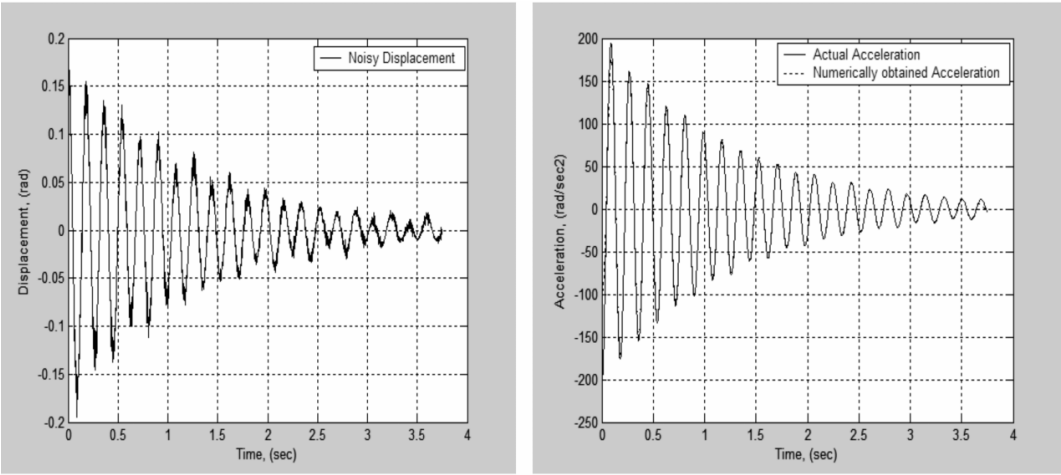

(a) Noisy displacement time-history (b) Generated acceleration time-history

Fig. 1 (a) Noisy displacement time-history (b) Generated acceleration time-history

which used only the middle portion of each of the three time histories for system identification. A 'window' that discards the first and last quarter of each time history was found suitable for obtaining parameters through system identification. Thus, only middle half of each time history is considered for extracting elements of the $\underline{A}$ matrix by the ILS approach.

The noise levels in the filtered displacement time history and numerically-generated velocity and acceleration time histories that is obtained from the filtered data are of concern. It is important to show that these noise levels are less than the noise in the displacement time history. This can be assessed only by numerical simulation since the noise level in any recorded time history is usually unknown. A displacement time history that is similar to the recorded one was generated and contaminated with Gaussian white noise where the noise-to-signal ratio was specified as 20%. The noisy displacement time history, as shown in Fig. 1(a), was then digitally filtered and used to generate velocity and acceleration time histories by finite difference formulation. The numerically-generated acceleration time history is shown Fig. 1(b). The error (in the same sense as noise to signal ratio defined in terms of RMS values) in the filtered displacement time history, as compared to the exact one, was calculated as 2.58%; the errors in the generated velocity and acceleration time histories, as compared to the exact ones, were calculated as 2.54% and 2.58%. This exercise proved that the noise in the numerically obtained velocity and acceleration time histories from a filtered displacement record is less than the one that are expected if these were measured values (assuming similar noise levels as in the displacement record).

The $\underline{A}$ matrix obtained for zero wind case will give the $\underline{C}^{mech}$ and $\underline{K}^{mech}$ matrices. The $\underline{A}$ matrix obtained for non-zero wind speeds will give the $\underline{C}^{eff}$ and $\underline{K}^{eff}$ matrices. After estimating the elements of these matrices, the frequency-dependent flutter derivatives are calculated. Based on the ILS approach, a computer code has been developed to identify the elements of $\underline{A}$ matrix from noisy displacement time histories. The algorithm of ILS approach is presented here as follows.

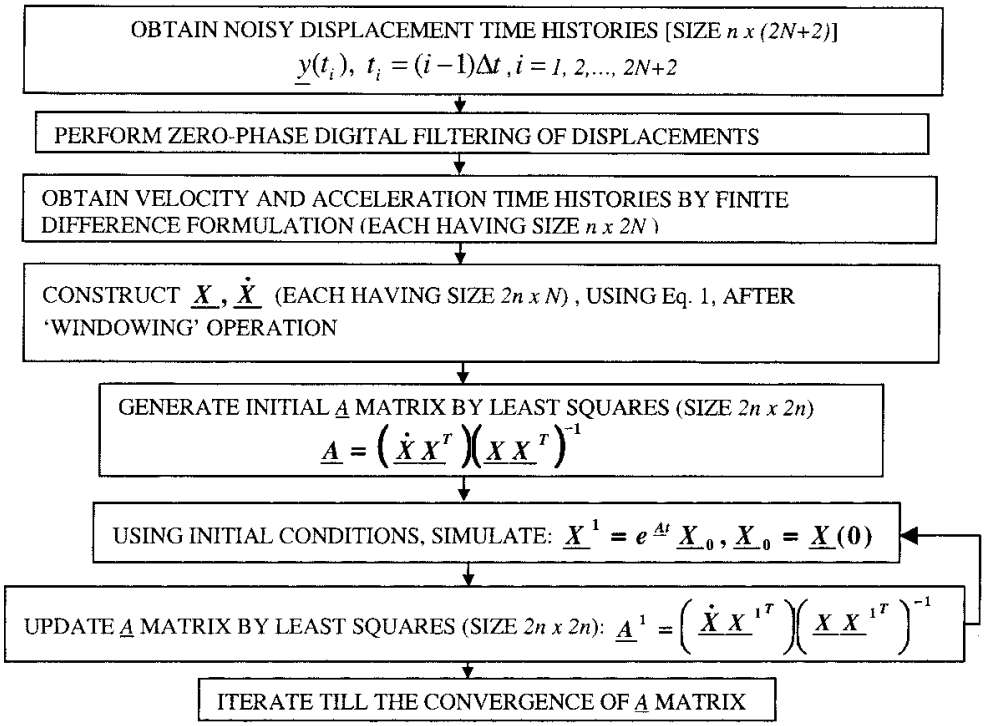

3. Experimental setup

3.1. Component description and assembly of the elastic suspension system

A three-DOF elastic suspension system (Fig. 2) has been developed and built for testing at the Wind Simulation and Testing (WiST) Laboratory, Department of Aerospace Engineering, Iowa State University. This system enables simultaneous vertical, horizontal, and torsional motion of the suspended model. The schematic diagram of the system is shown in Fig. 3. Extensive details of this suspension system can be found in Sarkar, Gan Chowdhury, and Gardner (2004).

The system comprise of six cylindrical-pneumatic bushing assemblies supported by six polished steel shafts – three bushing assemblies and three shafts at each end of the system; two bushing assemblies on two parallel vertical shafts and one bushing assembly on a horizontal shaft. Each end of the horizontal shaft is attached to a vertical bushing.

The suspension system uses extension springs, as shown in Fig. 3, for allowing the section model to vibrate in vertical and lateral directions. Extension springs, with particular configurations, were chosen to undergo large deflections.

The torsional motion of the system is generated using a torsional-assembly (Fig. 3) on either side of the system. Each torsional-assembly uses a pair of extension springs for allowing the rotational motion. The axis of the section model, which is a circular shaft, is supported by a high precision ball bearing mounted on the front wall of each torsional-assembly. The shaft is then connected to a rotating block. A solid aluminum rod runs through the rotating block. The pair of extension springs

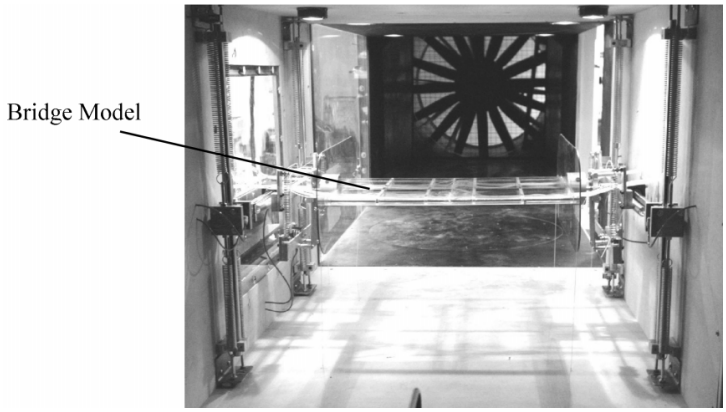

Fig. 2 Three-DOF elastic suspension system with streamlined bridge deck model B1

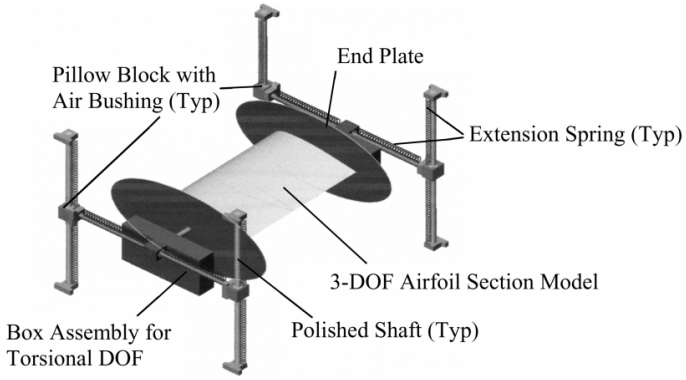

Fig. 3 Schematic diagram of three-DOF elastic suspension system

is connected to a rigid bar at the bottom and the solid aluminum rod at the top that can undergo oscillatory motion. The distance between the extension springs can be adjusted to vary the torsional stiffness of the system. The torsional-assemblies allow the model to undergo rotational motion under wind loading and the torque-sensor measures the elastic moment.

3.2. Elastic force and torque measurement system

The elastic spring force generated as a result of linear vertical or lateral motion needs to be measured to get the displacement time histories. These force measurements are accomplished with strain gage force transducers applied to four of the spring attachment points at the end of the polished shafts, two vertical (out of a maximum of sixteen springs) and two horizontal (out of a maximum of four springs). In the current studies, miniature load cells with 111 N (25 lb) capacities were used as force transducers.

For measuring the elastic moment proportional to the generated torsional motion, a torque-sensor is fixed to the back wall of one of the two torsional-assemblies. The front end of the torque sensor is connected to the rigid bottom bar, and thus it can measure the torque produced by the pair of

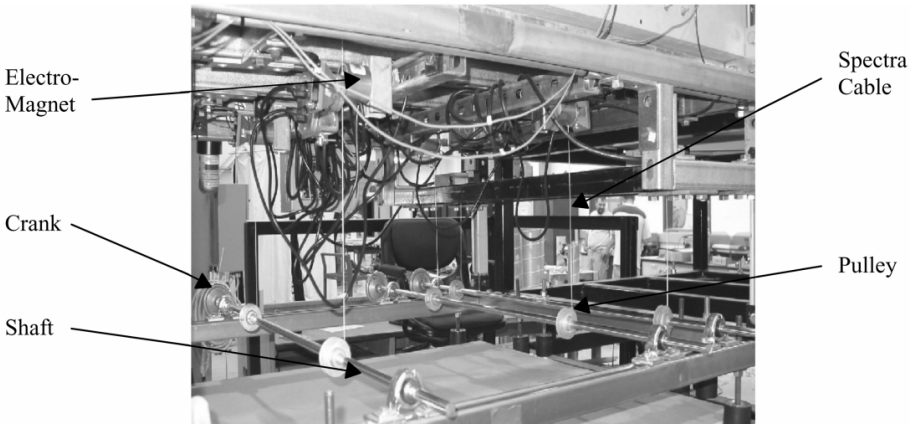

Fig. 4 Electromagnetic system for initial conditions

springs. A low-capacity light-weight torque sensor with a capacity of 11.29 N-m (100 lb-in.) was used for the experiments.

3.3. Electromagnetic system for initial conditions

An electromagnetic system (Fig. 4) is designed to provide desired initial displacement conditions to the model and then release it to undergo oscillatory motions. The initial conditions are provided through high strength thin spectra cables. Six cables (three on each side of the system) are used to generate the initial conditions. One end of each cable is connected to the model end plate and the other end is wrapped around a pulley fixed on an aluminum shaft. Cranks are used for rotating the shafts to pull down the cables by specific amounts. Thus, a model can be displaced to a position such that the desired initial conditions are imposed. Each cable is then clamped between a plate and an electromagnet. All the cables are clamped to attain the initial conditions. A single switch is used to turn off all the magnets simultaneously to allow the model to vibrate starting from the initial displaced position.

3.4. Airfoil and bridge deck section models

For wind tunnel testing, a NACA 0020 airfoil section model (Fig. 3) and a streamlined bridge deck section model (Fig. 5) were used. The airfoil was symmetric about its chord and had a maximum thickness-to-chord ratio of twenty percent. The center-of-gravity of the airfoil model was

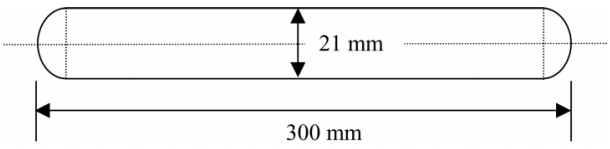

Fig. 5 Cross-section of bridge B1 (not to scale)

purposely coincided with the elastic axis to avoid static imbalance. The bridge deck model represented a shallow box girder section with semi-circular fairings for the edges. The thickness-to-chord ratio was seven percent for the bridge model. Each model was about 0.6 m long with a chord length of 0.3 m. Two *Plexiglas* end plates were used to reduce aerodynamic end effects for both models.

4. Results and discussions

4.1. Numerical simulations

The purpose of the numerical simulation was to determine the percentage of error for the elements of the damping and stiffness matrices, which were extracted from noisy displacement time histories. ILS method was programmed and tested for one, two, and three-DOF dynamic systems whose mass, stiffness, and damping matrices were assumed. Cases with different noise-to-signal ratios were considered during numerical simulation. The average errors for the stiffness and damping terms for two-DOF and three-DOF dynamic systems are given in Table 1.

The errors in diagonal terms are less compared to the errors in non-diagonal terms for the stiffness and damping matrices. The parameter errors increased with increasing noise level. Also, errors increased with increasing number of degree of freedom. Thus, it is recommended to generate all the eighteen flutter derivatives from different two-DOF combinations instead of performing a single three-DOF testing. The current method is capable of generating good estimates of parameters even for high noise-to-signal ratio for two-DOF systems (e.g., maximum error in extracted parameters is $\approx$5% for 20% noise level).

4.2. Experimental results

Eighteen flutter derivatives were obtained for the NACA 0020 airfoil model and the streamlined bridge model by using the ILS approach. The versatility of the three-DOF elastic suspension system remains in the fact that all possible two-DOF combinations could be tested in the wind tunnel. Since the three-DOF test proved to be more challenging and less accurate as shown in numerical simulations, three different sets of two-DOF testing, namely, vertical-torsional, vertical-lateral, and lateral-torsional, were performed to extract all the eighteen flutter derivatives.

A sampling rate of 800 Hz was used. The data points of the decaying sinusoidal motions that were below a certain amplitude were discarded during analysis to avoid high noise-to-signal ratio. An ensemble of ten displacement records was taken at each wind speed. The ILS program was used

Table 1 Average percentage errors* for numerical simulations

Case	Noise-to-Signal Ratio	Diagonal Stiffness Terms	Non-Diagonal Stiffness Terms	Diagonal Damping Terms	Non-Diagonal Damping Terms
2-DOF (ILS)	10%	0.06	0.82	0.56	1.41
2-DOF (ILS)	20%	0.13	0.96	2.01	5.04
3-DOF (ILS)	10%	0.89	2.34	4.83	8.43

*Average percentage error $= \frac{1}{M}\Sigma|X_i - Y_i| \times 100/Y_i$, where X_i is estimated value, Y_i is exact value, i = 1 to M and M is number of terms that is considered for averaging.

for processing the data. The cut-off frequency of the Butterworth filter was chosen slightly higher than the maximum zero-wind speed natural frequency of the dynamic system (i.e., around 4 Hz associated with the torsional motion of both the models). Any cut-off frequency chosen between 5 to 6 Hz was found to work effectively for filtering purposes. Finite difference formulation (central-difference with truncation error of $O[(\Delta t)^2]$) was used to obtain the velocity and acceleration time

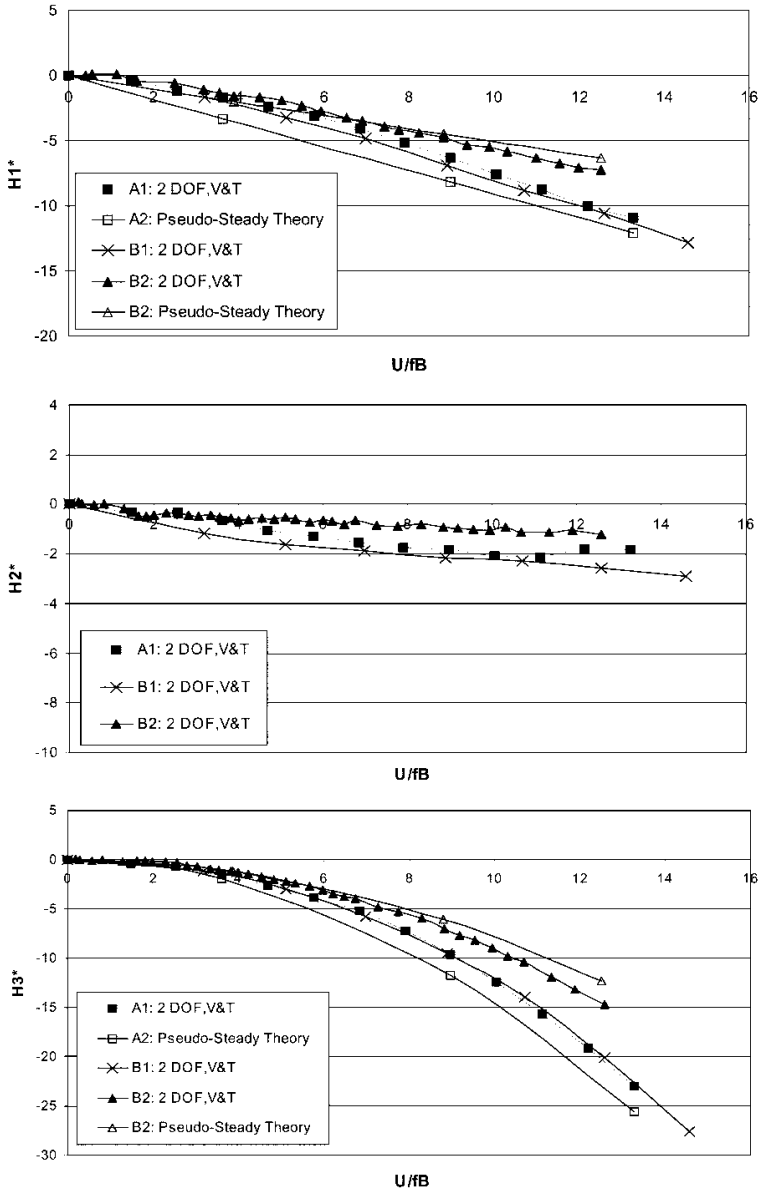

(a) Vertical flutter derivatives (H_i^*, i=1,2,3)

Fig. 6 (a) Vertical flutter derivatives (H_i^*, i=1, 2, 3)

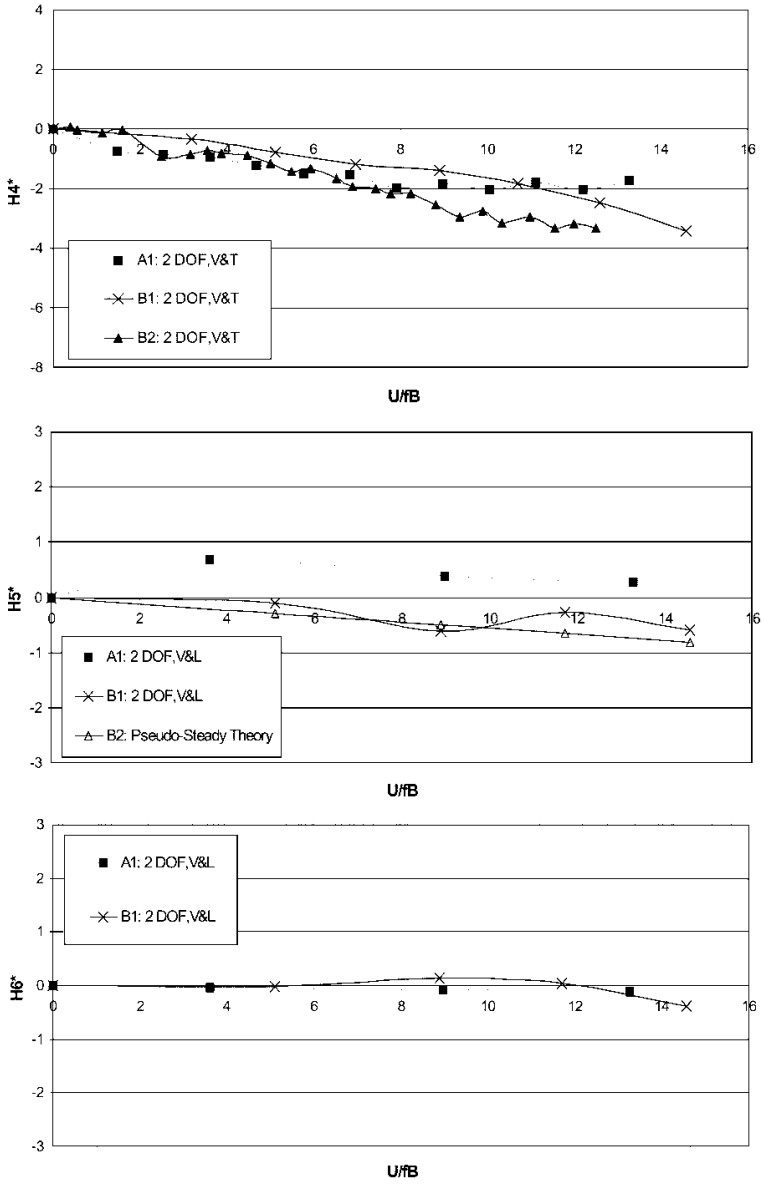

(b) Vertical flutter derivatives (H_i^*, i=4,5,6)

Fig. 6 (b) Vertical flutter derivatives (H_i^*, i=4, 5, 6)

histories from the digitally filtered displacement data.

In the experiments presented here, flutter derivatives were obtained from different DOF combinations (V: vertical; T: torsional; L: lateral) for a NACA 0020 airfoil and a streamlined bridge deck as described earlier. The zero-wind vertical frequency of the dynamic system was used to obtain the non-dimensional reduced velocity for all these cases. However, for a comparative study, flutter derivatives of another airfoil (NACA 0018) and two other streamlined bridge deck models are used. These models are numbered as follows for future reference:

A1: Current NACA 0020 airfoil with a maximum thickness-to-chord ratio of 20%
A2: NACA 0018 airfoil with a maximum thickness-to-chord ratio of 18% (data for this airfoil is obtained from Blevins 1992 because it is similar to A1)
B1: Current streamlined bridge deck with semicircular fairings and thickness-to-chord ratio of 7%
B2: Streamlined bridge deck with tapered edges and thickness-to-chord ratio of 9.6% (Tsurumi bridge – single-deck configuration, Sarkar, Jones, and Scanlan 1994)

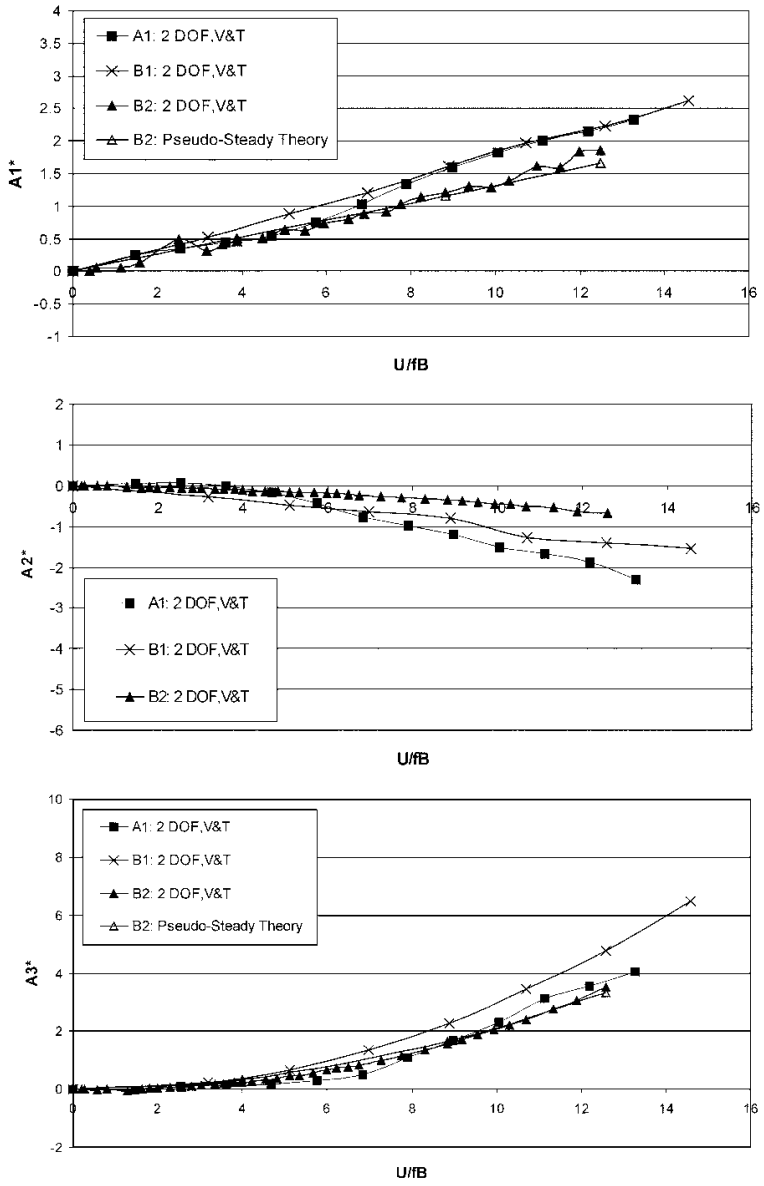

(a) Torsional flutter derivatives (A_i^*, i=1,2,3)

Fig. 7 (a) Torsional flutter derivatives (A_i^*, i=1,2,3)

B3: Streamlined bridge deck with tapered edges and thickness-to-chord ratio of 9.8% (model '*a*' from Chen, He, and Xiang 2002).

The flutter derivatives are plotted in Figs. 6 to 8. For the current bridge deck (B1), good agreement is seen for direct lateral flutter derivatives ($P1^*$, $P4^*$) obtained from different two-DOF combinations, thus showing the consistency of experimental results (refer Eq. (2) for definition of flutter derivatives in three-DOF formulation). The lateral derivative $P1^*$ for the current bridge deck, which represents the damping of lateral displacement, has a steeper slope than that of the NACA

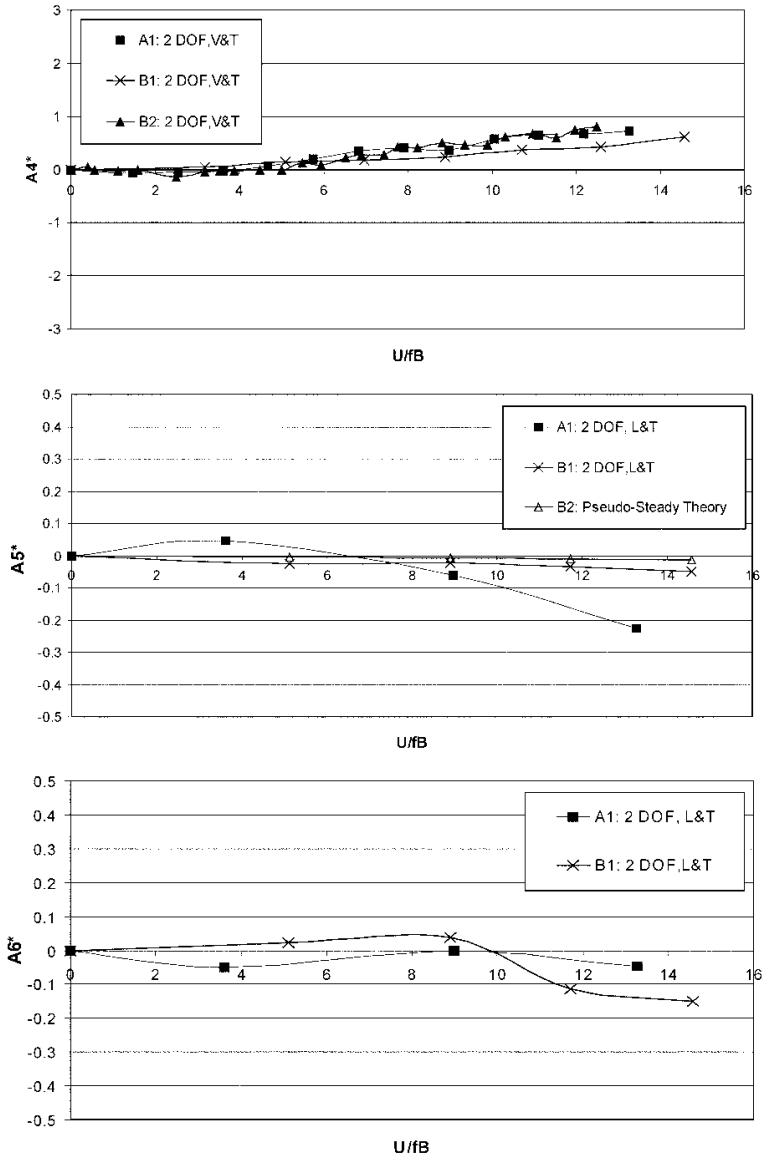

(b) Torsional flutter derivatives (A_i^*, i = 4,5,6)

Fig. 7 (b) Torsional flutter derivatives (A_i^*, i=4,5,6)

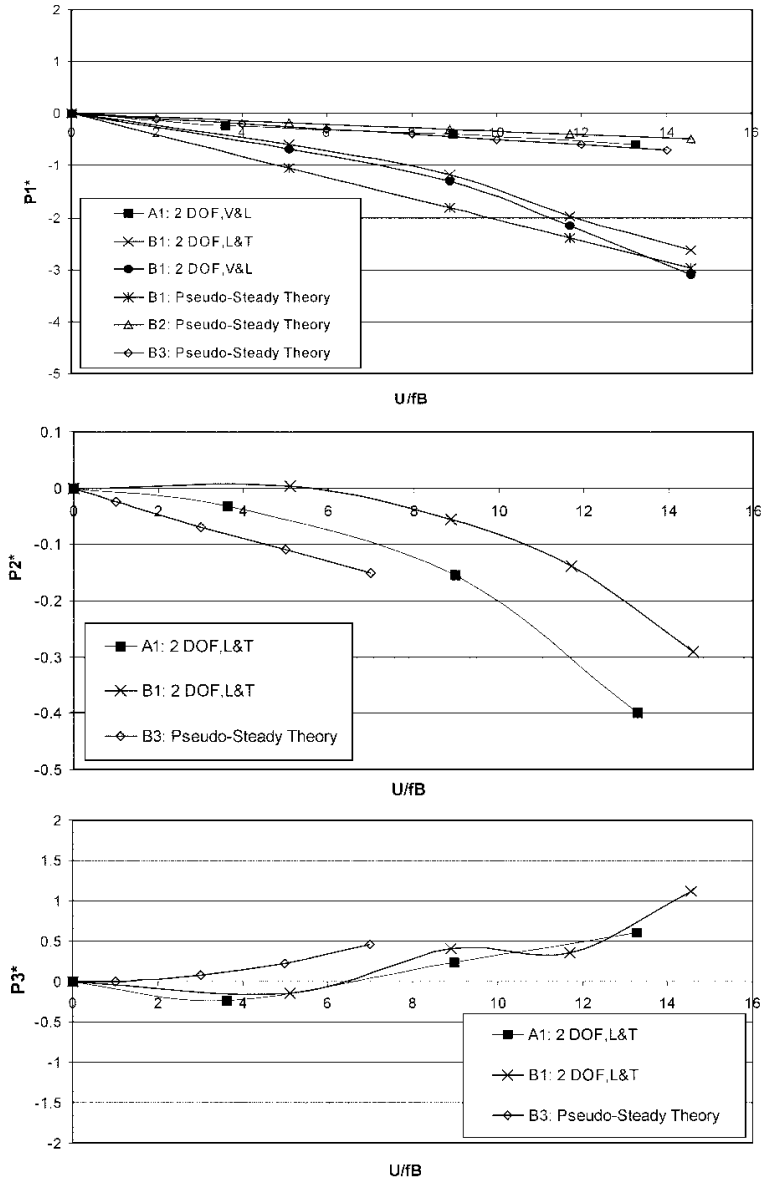

(a) Lateral flutter derivatives (P_i^*, i = 1, 2, 3)

Fig. 8 (a) Lateral flutter derivatives (P_i^*, i=1, 2, 3)

0020 airfoil (A1) suggesting that higher lateral damping rate is associated with the bridge deck model as compared to the airfoil model. Also, as opposed to the airfoil model case (A1), distinct trend is noted for $P4^*$ of 'B1', which represents the frequency of lateral displacement, suggesting monotonic increase in lateral displacement frequency with wind speed. For other experimental lateral derivatives, similar trends are noted for the airfoil (A1) and bridge deck (B1). For the Tsurumi bridge deck section model (B2) and the current bridge deck section model (B1), similar

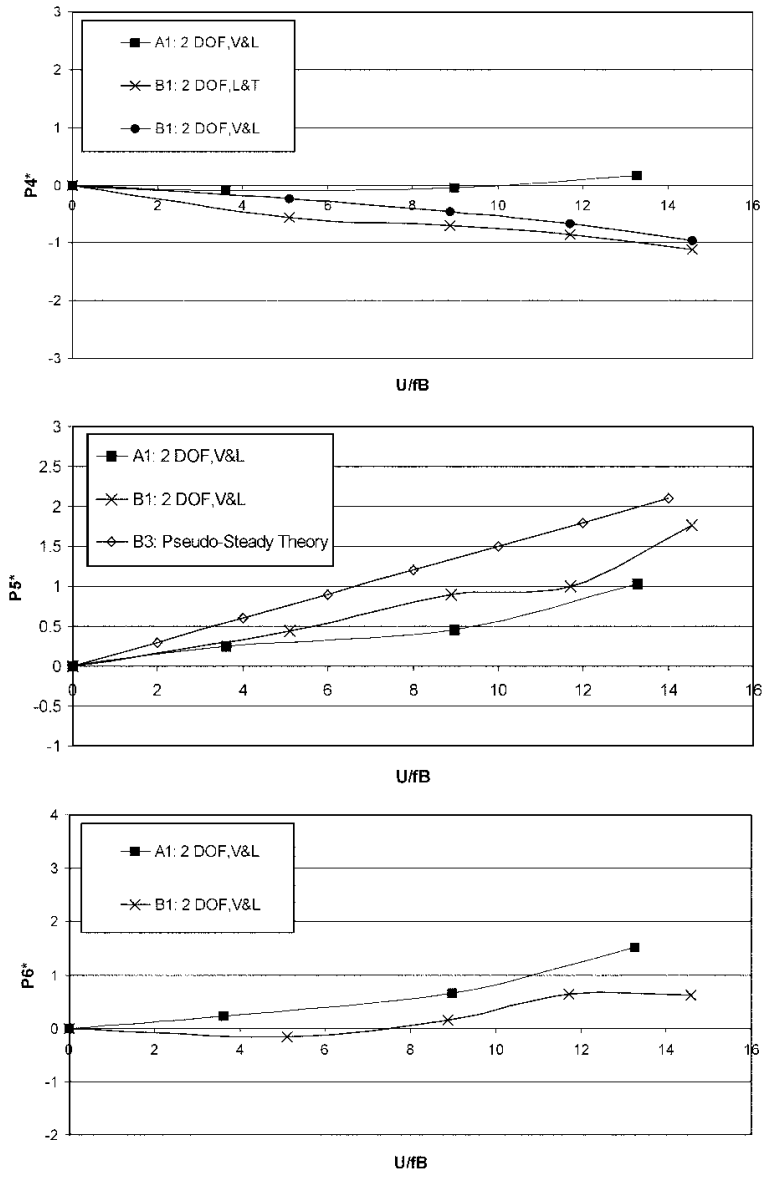

(b) Lateral flutter derivatives (P_i^*, i=4,5,6)

Fig. 8 (b) Lateral flutter derivatives (P_i^*, i=4,5,6)

trends have been found for the vertical and torsional flutter derivatives $H1^*$, $H2^*$, $H3^*$, $H4^*$, $A1^*$, $A2^*$, $A3^*$, $A4^*$.

4.3. Pseudo-steady formulation

Pseudo-steady formulation for $P1^*$, $P2^*$, $P3^*$ are given by Scanlan (1987) as:

$$P_1^* = -\frac{2}{K}C_D;\quad P_2^* = \frac{1}{K}\frac{dC_D}{d\alpha_w};\quad P_3^* = \frac{1}{K^2}\frac{dC_D}{d\alpha_w} \tag{3}$$

The pseudo-steady formulation for P1*, P3*, P5*, H1*, H3*, H5*, A1*, A3*, A5*, as derived independently by the co-authors, are presented here:

$$P_1^* = -\frac{2}{K}C_D;\quad P_3^* = \frac{1}{K^2}\frac{dC_D}{d\alpha_w};\quad P_5^* = \frac{1}{K}\left(\frac{dC_D}{d\alpha_w} - C_L\right);$$

$$H_1^* = -\frac{1}{K}\left(\frac{dC_L}{d\alpha_w} + C_D\right);\quad H_3^* = -\frac{1}{K^2}\frac{dC_L}{d\alpha_w};\quad H_5^* = \frac{2}{K}C_L;$$

$$A_1^* = \frac{1}{K}\frac{dC_M}{d\alpha_w};\quad A_3^* = \frac{1}{K^2}\frac{dC_M}{d\alpha_w};\quad A_5^* = -\frac{2}{K}C_M \tag{4}$$

Chen, He, and Xiang (2002) also presented the pseudo-steady formulation for P1*, P2*, P3*, P5*, H5*, A5*. These formulae can be modified and re-written to match the flutter-derivative convention of Scanlan, Jones and co-workers. The formulae for P1*, P3*, P5*, H5*, A5* given in Eq. (4) match with these modified forms, whereas P2* is given as

$$P_2^* = -\frac{1}{4K}\left(\frac{dC_D}{d\alpha_w} - C_L\right) \tag{5}$$

In Eqs. (3-5), C_D, C_L, C_M are the static drag, lift, and moment coefficients, respectively, and α_w is the angle of incidence of the wind. Static coefficients were not measured for the current bridge deck model. Static drag coefficient of the current bridge section (B1) was assumed as 0.64 based on Blevins' data (Blevins 1992) for a thin rectangular section with a semicircular leading edge and an aspect ratio of 6.0. Thus, only pseudo-steady P1* for 'B1' is plotted. Using the static coefficients of the single-deck configuration of Tsurumi bridge (B2), given by Sarkar (1992) as $C_D = 0.104$, $C_L = -0.176$, $C_M = 0.003$, $dC_L/d\alpha_w = 3.100$, $dC_M/d\alpha_w = 0.832$, its flutter derivatives H1*, H3*, H5*, A1*, A3*, A5*, P1* are plotted based on Eq. (4). P2*, P3* and P5* of B2 could not be calculated since $dC_D/d\alpha_w$ was not known. Also, based on the pseudo-steady formulation, flutter derivatives P1*, P2*, P3*, P5* are plotted for another streamlined bridge deck (B3) as given by Chen, He, and Xiang (2002). Pseudo steady H1* and H3* are plotted for a NACA 0018 airfoil (A2) based on available static coefficient values, $C_D = 0.01$ and $dC_L/d\alpha_w = 5.73$ (Blevins 1992). In the following comparisons, it should be noted that 'A1' and 'A2' are airfoils with almost same thickness-to-chord ratios and 'B1', 'B2' and 'B3' are all streamlined decks with similar aspect ratios.

For bridge 'B2', experimental H1*, H3*, A1*, A3* matched very well with their pseudo-steady counterparts, thus validating the pseudo-steady formulation for these flutter derivatives as presented in the current paper. Also, experimental H1* and H3* for airfoil 'A1' are in agreement with the pseudo-steady plots for airfoil 'A2'.

H5* and A5* of bridge 'B2' (not originally obtained by Sarkar 1992) based on pseudo-steady theory have good agreement with the experimentally obtained plots for bridge 'B1'.

Trends of P2*, P3*, P5* for bridge 'B3', based on the pseudo-steady formulation, match with those experimentally obtained for bridge 'B1'. For P1*, the pseudo-steady plots for bridges 'B2' and 'B3' agree well with that of the airfoil 'A1'. For bridge 'B1', the experimental P1* plot shows a

comparatively steeper slope. This particular phenomenon could be caused as a result of higher drag coefficient generated by semi-circular fairings of the current bridge deck that are relatively more bluff compared to the tapered edges of 'B2' and 'B3'. As mentioned earlier, the static drag coefficient of 'B1' was assumed based on Blevins' data for a section with semicircular edge. The pseudo-steady plot thus obtained for $P1^*$ shows good agreement with the experimentally obtained $P1^*$ for 'B1'. The overall agreement of the experimental and the pseudo-steady theory based flutter derivatives bolsters the pseudo-steady formulation given in the current paper.

5. Conclusions

Eighteen flutter derivatives for an airfoil section model and a streamlined bridge deck model were extracted using a new system identification method (ILS method). There is consistency in the values of flutter derivatives that were obtained from more than one set of DOF combination (only comparison for direct lateral flutter derivatives is shown here). The vertical and torsional flutter derivatives ($H1^*$, $H2^*$, $H3^*$, $H4^*$, $A1^*$, $A2^*$, $A3^*$, $A4^*$) for the airfoil, A1, and bridge deck, B1, have similar trends. Also, comparison with the two-DOF flutter derivatives of Tsurumi bridge deck model (single-deck configuration) shows that the trends are similar with those for the current bridge model. The lateral derivatives $P1^*$ and $P4^*$ differed for the airfoil and current bridge model and their significances are discussed. Pseudo-steady formulation for $P1^*$, $P2^*$, $P3^*$, $P5^*$, $H1^*$, $H3^*$, $H5^*$, $A1^*$, $A3^*$, $A5^*$ are discussed. Bridge deck flutter derivatives, obtained from both experiments and pseudo-steady theory, are compared to validate the pseudo-steady formulation.

References

Blevins, R.D. (1992), *Applied Fluid Dynamics Handbook*, Krieger Publishing Company, Malabar, Florida.

Brownjohn, J.M.W. and Jakobsen, J.B. (2001), "Strategies for aeroelastic parameter identification from bridge deck free vibration data", *J. Wind Eng. Ind. Aerod.*, **89**, 1113-1136.

Chen, A., He, X. and Xiang, H. (2002), "Identification of 18 flutter derivatives of bridge decks", *J. Wind Eng. Ind. Aerod.*, **90**, 2007-2022.

Gan Chowdhury, A. and Sarkar, P.P. (2003), "Identification of eighteen flutter derivatives", *Proc. the 11th International Conference on Wind Engineering*, Lubbock, Texas, June.

Gu, M., Zhang, R. and Xiang, H. (2000), "Identification of flutter derivatives of bridge decks", *J. Wind Eng. Ind. Aerod.*, **84**, 151-162.

Ibrahim, S.R. and Mikulcik, E.C. (1976), "The experimental determination of vibration parameters from time responses", *The Shock and Vibration Bulletin*, **46**, 187-196.

Sarkar, P.P. (1992), "New-identification methods applied to the response of flexible bridges to wind", PhD Thesis, The Johns Hopkins University, Baltimore, MD.

Sarkar, P.P., Jones, N.P. and Scanlan, R.H. (1994), "Identification of aeroelastic parameters of flexible bridges", *J. Eng. Mechanics*, ASCE, **120**(8), 1718-1742.

Sarkar, P.P., Gan Chowdhury, A. and Gardner, T.B. (2004), "A novel elastic suspension system for wind tunnel section model studies", *J. Wind Eng. Ind. Aerod.*, **92**, 23-40.

Scanlan, R.H. (1978), "The action of flexible bridges under wind, I: flutter theory", *J. Sound Vib.*, **60**(2), 187-199.

Scanlan, R.H. (1987), "Interpreting aeroelastic models of cable-stayed bridges", *J. Eng. Mechanics Div.*, ASCE, **113**(4), 35-55.

Singh, L., Jones, N.P., Scanlan, R.H. and Lorendeaux, O. (1995), "Simultaneous identification of 3-dof aeroelastic parameters", *Proc. the 9th International Conference on Wind Eng.*, New Delhi, India.

Zhu, L.D., Xu, Y.L., Zhang, F. and Xiang, H.F. (2002), "Tsing Ma bridge deck under skew winds - Part II: flutter derivatives", *J. Wind Eng. Ind. Aerod.*, **90**, 807-837.

CC